Materials Advances

ROYAL SOCIETY OF CHEMISTRY

COMMUNICATION

View Article Online
View Journal | View Issue

Open Access Article. Published on 11 January 2022. Downloaded on 6/9/2026 3:33:48 PM.
This article is licensed under a Creative Commons Attribution-NonCommercial 3.0 Unported Licence.

Check for updates

Cite this: *Mater. Adv.*, 2022, 3, 1518

Received 18th December 2021,
Accepted 11th January 2022

DOI: 10.1039/d1ma01200b

rsc.li/materials-advances

Novel TiO_2/TPU composite fiber-based smart textiles for photocatalytic applications†

Jing Zhang,[a] Xuan Li,[a] Jian Guo,[b] Gengheng Zhou,[cd] Li Xiang,[e] Shuguang Wang[a] and Zuoli He *[a]

Herein, we prepare a novel hollow composite fiber *via* a wet-spinning process to overcome the nanostructured catalysts' separation and recovery problems. The obtained TiO_2/TPU fiber showed excellent mechanical and photocatalytic performance. The fiber-based textile achieved 99.6% degradation efficiency of rhodamine B (RhB) and a high hydrogen production rate of 81.75 μmol g^{-1} h^{-1}.

Introduction

Since Hoda and Fujishima investigated water splitting into oxygen and hydrogen by TiO_2 under UV light irradiation, many intricate nanostructured and heterogeneous photocatalysts have been reported with high photocatalytic performances.[1–6] Currently, TiO_2 photocatalysis is actively used in the field of photodegradation of organic compounds, specifically in environmental decontamination of wastewater, which also suffers from some problems.[7–11] During practical application, photocatalysts exist as a powder in the water system, ensuring a high number of photoactive sites and optimizing mass transfer.[12] However, nanophotocatalysts also have some drawbacks. Due to their relatively small size, suspended photocatalysts tend to rapidly aggregate, considerably decreasing their effective surface area and catalytic efficiency.[13–17] Moreover, the fate and transportation of the dispersed powder are closely related to potential human health problems.[18] Therefore, it is an urgent but challenging need to separate and collect nanoparticles from the solution system and improve their stability for continuous use.[19,20] Current concerns about nanostructured photocatalysts include overcoming separation and recovery problems from solutions during practical applications, such as stability, toxicity, and secondary pollution, to improve the applicability. Developments of these practical applications are of significant potential industrial and scientific importance and require considerable effort and time.

Many researchers have focused their attention on the immobilization of TiO_2 nanoparticles on different support materials to improve the photocatalytic activity and separate them more effectively. Some common examples of such support materials include glass, activated carbon, silica, polymers, plant fibers, *etc.*[15,21–23] Nevertheless, the entrapment of these nanoparticles on an inert substrate provides an inherent drawback of losing a portion of the surface-active sites, which will reduce the activity of photocatalysts and enlarge the mass transfer limitations. Additionally, immobilization of the catalysts results in an increased operational difficulty, as the light will not be able to effectively reach the surface-active sites of the catalyst, thereby reducing photonic activation. Moreover, most of the support materials are either expensive, contain potential impurities, or display reduced durability and flexibility.[24] Due to their low cost, chemical inertness, mechanical stability and high durability, polymer supports have been demonstrated to be among the best candidate materials for the immobilization of photocatalyst nanoparticles. Polymers with functional properties, such as self-healing, response to stimuli, biodegradability or electrical conductivity, play a significant role in industry and daily life. The combination of traditional polymers with nanophotocatalysts is highly worthwhile for the improvement of practical application through photocatalytic engineering. In addition, polymer supports have a relatively low density, making it easy to design floating photocatalysts, especially in aqueous media.[25–27] Thermoplastic polyurethane (TPU) is an elastomer with low-temperature flexibility, biocompatibility, resistance to hydrolysis, optical transparency, flame retardancy and antistatic properties.[28] In particular, the incorporation of

[a] *Shandong Key Laboratory of Water Pollution Control and Resource Reuse, School of Environmental Science and Engineering, Shandong University, Qingdao 266237, China*
[b] *China Academy of Launch Vehicle Technology, Beijing 100076, China*
[c] *Suzhou Institute of Nano-Tech and Nano-Bionics, Chinese Academy of Sciences, Suzhou 215123, China*
[d] *Gusu Laboratory of Materials, Gusu Laboratory of Materials, Suzhou 215123, China*
[e] *Department of Chemistry, Pohang University of Science and Technology (POSTECH), Pohang, 37673, Republic of Korea*

† Electronic supplementary information (ESI) available. See DOI: 10.1039/d1ma01200b

© 2022 The Author(s). Published by the Royal Society of Chemistry

Open Access Article. Published on 11 January 2022. Downloaded on 6/9/2026 3:33:48 PM.
This article is licensed under a Creative Commons Attribution-NonCommercial 3.0 Unported Licence.

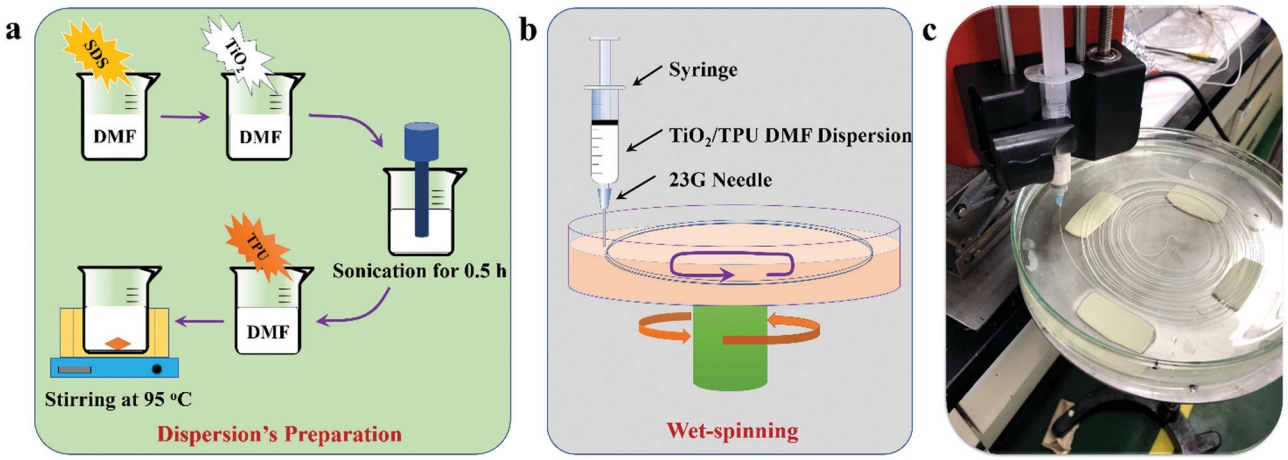

Scheme 1 Schematic illustration (a and b) and image (c) of the wet spinning process.

TPU could improve the overall durability of products.[29] Several property combinations of TPU make it suitable for many applications, such as catalyst supports and sensors, and in the automotive, footwear, and construction industries.[28,30–34] In addition, the recycling processes of TPU have been reported to be economical and practical.[35] Thus, compared with other conventional polymers, TPU is an excellent material for the immobilization of photocatalyst nanoparticles. Recently, stretchable composite fibers have gained significant attention owing to their ability to be directly woven into or stitched onto textiles.[36–39] In such a composite fiber system,

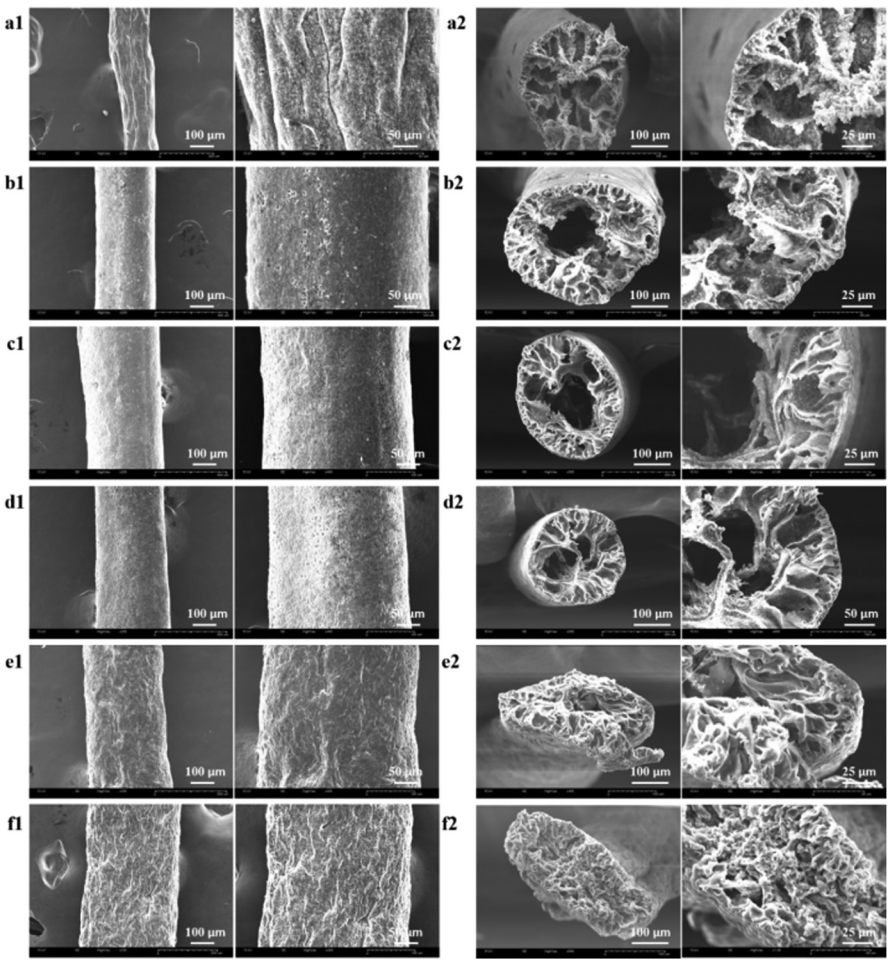

Fig. 1 (a1–e2) SEM images of as-prepared fibers which TiO_2 : TPU was 1 : 2, 1 : 5, 1 : 8, 1 : 12, 1 : 20, respectively; (f1 and f2) SEM images of neat TPU fiber.

Open Access Article. Published on 11 January 2022. Downloaded on 6/9/2026 3:33:48 PM.
This article is licensed under a Creative Commons Attribution-NonCommercial 3.0 Unported Licence.

polymer matrix materials could introduce superior stretchability, and functional elements in the polymer matrix could modify and/or increase the functionality of fibers. So, composite fiber will process the unique properties for various practical applications, such as energy devices, optics, sensors, microelectronics, catalytic devices, *etc.* These qualities will provide better wearability and integrality for the practical application of photocatalysis.[40,41]

In that sense, TiO_2 NPs should be exposed on the surface as much as possible during immobilization in the TPU matrix. Hollow fibers with a larger surface area were a better choice to prepare such functional composite fibers. Therefore, we prepared a novel hollow TPU-based composite fiber *via* a wet-spinning process by immobilizing TiO_2 nanoparticles in its matrix as shown in Scheme 1.[42] In this system, we used flexible and durable TPU to introduce superior stretchability, and TiO_2, which acts as a functional filler for photocatalysis. First, we investigated the effect of TiO_2 content on the structure and mechanical performance of the composite fibers. Then, the TiO_2/TPU hollow composite fiber was woven into a textile to evaluate its photocatalytic performance. To assess the quality of the TiO_2/TPU fiber, its tensile properties were investigated. Moreover, the fiber was braided into a textile to evaluate its photocatalytic performances (including degradation and hydrogen production) and stability.

Results and discussions

The surface morphologies of the as-prepared composite and neat TPU fibers were investigated using scanning electron microscopy (SEM). As shown in Fig. 1a1–2, the 1 : 2 TiO_2/TPU fiber with diameters of 150–240 μm presents a rough surface, indicating that a much higher catalyst content does not benefit the formation of uniform fibers in our experiments. At high concentrations, the agglomeration of TiO_2 NPs by the strong van der Waals force results in the formation of dense networks in the TPU matrix. Fig. 1b1–f2 shows SEM images of 1 : 5, 1 : 8, 1 : 12, and 1 : 20 TiO_2/TPU fibers and neat TPU fibers. The TiO_2/TPU composite fiber shows a hollow structure when the mass ratio of TiO_2 : TPU is lower than 1 : 5. This hollow structure enables more TiO_2 to be exposed on the surface of the fibers, which will be better for the photocatalytic process. The hollow porous structure is conducive to heterogeneous catalytic reactions, promoting the diffusion and transport of reactant molecules and may help to improve the photocatalytic activity. With decreasing TiO_2 content, the diameters of the holes in fibers decrease due to the decreasing supporting function of TiO_2. The 1 : 20 TiO_2/TPU and neat TPU fibers (Fig. 1f1–2) exhibited a porous microstructure with folds on their surface. The fibers were elliptical, which was related to the lower support from TiO_2 during TPU coagulation. A possible explanation for the formation of hollow fiber might be as follows: once the TiO_2/TPU spinning suspension is extruded into the coagulation solution, acetone diffuses into the fiber.[28] Simultaneously, the DMF in the fiber diffuses into the coagulation solution, and the surfactant dissolves as well. The fibers begin shrinking from the surface. The TiO_2 content influences the phase diffusion and coagulation rate, and it also determines the size and percentage of pores. At a high concentration of TiO_2, the agglomeration of TiO_2 NPs prevents the formation of large pores.[43–45] When the concentration decreases, TiO_2 NPs cannot

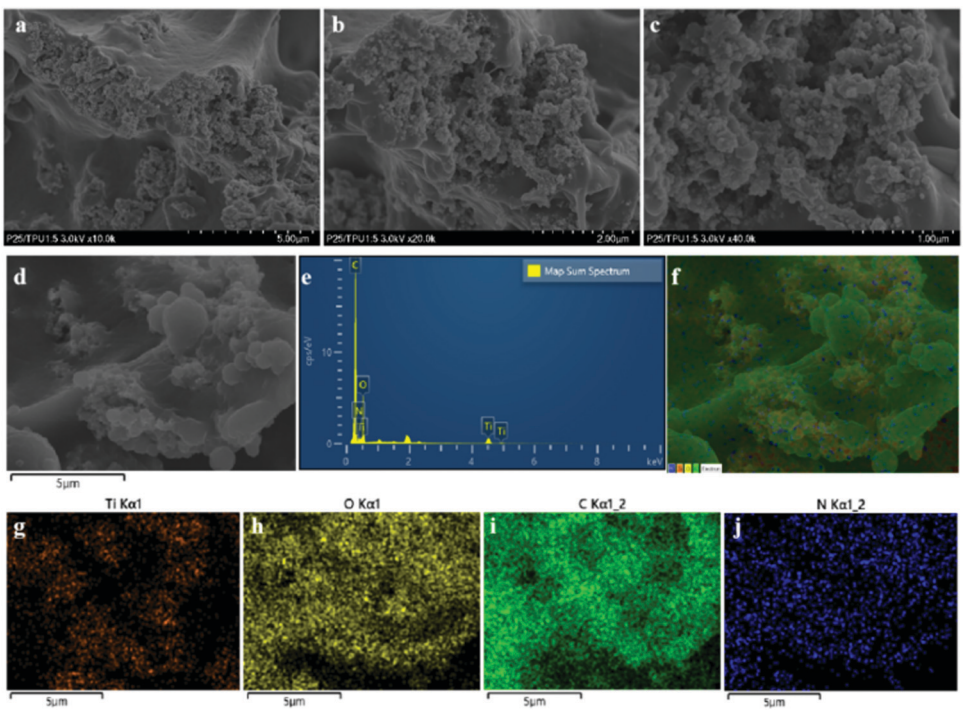

Fig. 2 (a–d) FE-SEM images; (e) EDX spectra; (f–j) element mapping images of 1 : 5 TiO_2 : TPU fiber.

© 2022 The Author(s). Published by the Royal Society of Chemistry

Open Access Article. Published on 11 January 2022. Downloaded on 6/9/2026 3:33:48 PM.
This article is licensed under a Creative Commons Attribution-NonCommercial 3.0 Unported Licence.

Table 1 EDX spectra results of 1 : 5 TiO2 : TPU fiber

Element	Line type	Wt%	Wt% Sigma	Atomic %
C	K series	57.83	0.60	68.79
N	K series	1.28	0.85	1.31
O	K series	29.78	0.42	26.59
Ti	K series	11.12	0.28	3.32
Total:		100.00		100.00

prevent the formation of large pores, so hollow pores will appear during coagulation from the surface to the interior. Interestingly, the 1 : 20 TiO_2/TPU and neat TPU fibers show an oval-shaped cross-section due to the lack of TiO_2 NPs. Injection through the spinneret and further elongation of fibers during the winding-up process give rise to the alignment of NPs exposed on the fiber surface. Furthermore, TPU long-chain molecules align more effectively along the spinning direction during the wet-spinning process, enabling superior stretchability for the preparation of smart textiles.[46]

The composite fiber was also analyzed using field emission scanning electron microscopy (FE-SEM) coupled with energy-dispersive X-ray spectroscopy (EDX) to observe the dispersion of TiO_2. It can be observed from the FE-SEM images of the TiO_2/TPU fiber (Fig. 2a–d) that most TiO_2 was exposed on the surface. The EDS spectrum and elemental mapping images (Fig. 2e–j) indicated the existence of Ti, O, C and N. Furthermore, TiO_2 was not distributed inhomogeneously in the fiber, but some TiO_2 aggregated. Table 1 shows the analyses of all elements, which further proved that no impurities existed in the fiber.

A filament tensile test was performed to investigate the mechanical properties of the composite fibers using a TA Instruments Q800 Dynamic Mechanical Analyzer (DMA). The fiber was pasted on a small piece of paper with a 20 mm × 5 mm hole in the center, and the hole was cut open after being fixed on the DMA before measurement. It should be noted here that the 1 : 2 TiO_2/TPU fiber is easily broken and could not be fixed in our small piece of paper for tensile test, due to the lower tensile strength and lowest failure strain resulting from too many TiO_2 inclosed in TPU matrix. The typical tensile strength–strain curves of the TiO_2/TPU and neat TPU fibers are shown in Fig. 3a–c. The tensile strength of the neat TPU fiber was ~49 MPa, with a maximum failure strain of 490%. With increasing TiO_2 content, the mechanical properties of the composite fiber decreased, regardless of the tensile strength or the maximum failure strain. The fiber with a weight ratio of 1 : 5 had the lowest tensile strength and minimum failure strain among all the composite fibers, which were ~9 MPa and ~322%, respectively. The decreased elongation at break in the composite fiber was attributed to the relatively poor interfacial contact with TPU and agglomeration of TiO_2, which affected the stretchability of the TPU matrix.[28] It should be noted that the composite fiber with higher filler content(higher than 1 : 5) does not present the hollow structure and easy break, so it could not be used for 20 mm filament tensile strength–strain measurement. Regardless, the 1 : 5 TiO_2/TPU fiber is better for building smart textiles for photocatalytic applications in our experiment due to its higher content of TiO_2 photocatalysts.

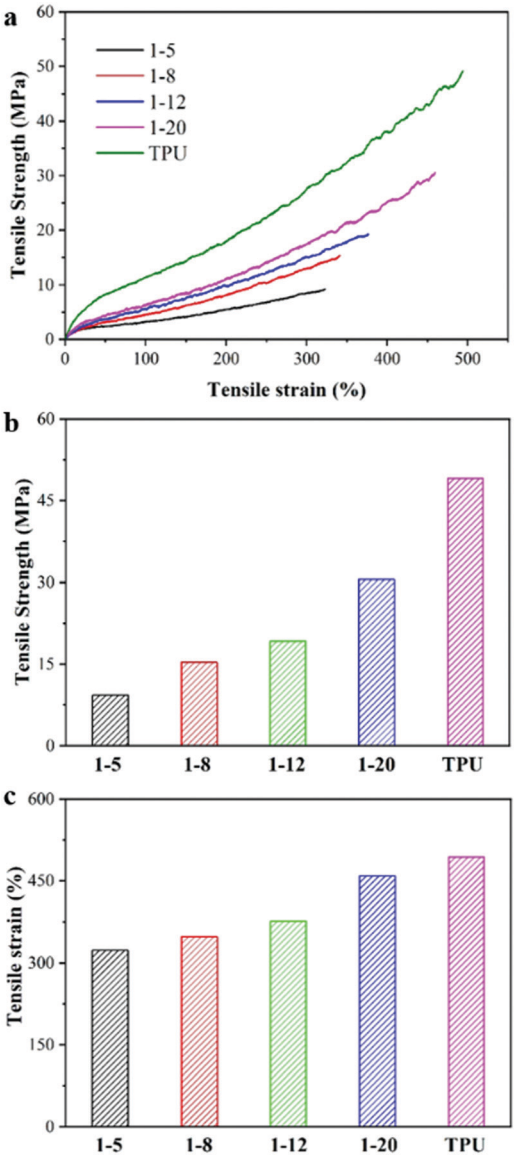

Fig. 3 (a–c) Tensile strength–strain curves of the TiO_2/TPU composite fibers.

As a ''green'' wastewater purification technology driven by solar radiation, photocatalysis has been widely used for decomposing organic pollutants into harmless inorganic molecules. As shown in Fig. 4, the TiO_2/TPU composite fiber was woven into a textile and fixed on a two-line stage to evaluate its photocatalytic performance, such as photodegradation and H_2 production (more details in ESI:† Fig. S1). The photodegradation performances of the TiO_2/TPU fiber-based textile were evaluated by removing RhB and 4-CP from an aqueous solution under light irradiation. The data were normalized to the same weight of the smart textile for comparison. Fig. 5a illustrates the adsorption and time-dependent photodegradation curves of

Open Access Article. Published on 11 January 2022. Downloaded on 6/9/2026 3:33:48 PM.
This article is licensed under a Creative Commons Attribution-NonCommercial 3.0 Unported Licence.

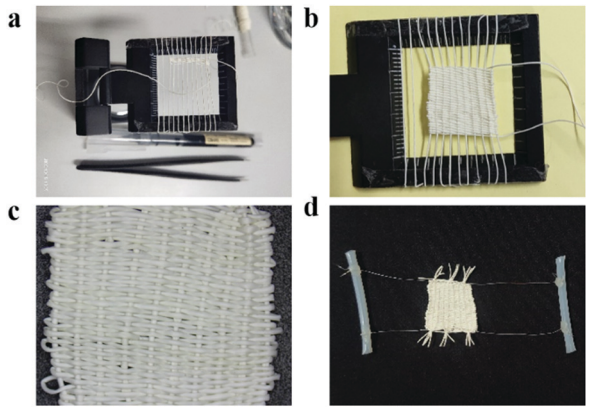

Fig. 4 The images of smart textiles for photocatalytic applications: (a) composite fiber woven into a textile; (b and c) the woven textile; (d) the fixed smart textiles for photocatalytic degradation and photocatalytic H_2 production.

5 ppm RhB over TiO_2/TPU fiber-based textiles with different TiO_2 contents. More TiO_2 in the fiber visibly improved the photodegradation performance. The porous hollow structures enabled more photocatalysts to be exposed on the fiber surface, which was beneficial to the contact of pollutants with photocatalysts, resulting in the excellent degradation performance of hollow fiber-based textiles. The hollow 1 : 5 TiO_2/TPU fiber-based textile showed the best photocatalytic performance, and the removal efficiency under light irradiation reached 99.6% after 240 min. In contrast, the 1 : 20 TiO_2/TPU fiber-based textile exhibited the worst photocatalytic performance, and the degradation efficiency decreased to 91.3% after 240 min irradiation. In addition, the effects of the initial RhB concentration on the degradation efficiency of hollow 1 : 5 TiO_2/TPU fiber-based textiles were investigated using different RhB concentrations (5, 10, 15, and 20 ppm). As shown in Fig. 5b, the degradation efficiency of RhB decreased from 99.6% to 75.6% as the initial RhB concentration increased from 5 to 20 ppm. This may be attributed to the fact that a higher concentration of RhB consumed more photogenerated reactive oxygen species. The stability of our smart textile was also vital to its practical applicability in photocatalysis. To confirm the stability of the TiO_2/TPU fiber-based textile, recycling experiments were carried out on the photodegradation of RhB in five cycles. As shown in Fig. 5c, after five cycles under the same conditions, the textile still maintained a high-efficiency degradation capacity. Moreover, the device exhibited the highest degradation capacity in the third cycle, which may be due to more TiO_2 exposure during the reaction. Textiles colored with RhB could also turn white in sunlight by self-cleaning as shown in Fig. S3 (ESI†), thus enabling the use of smart textiles for other applications, such as self-cleaning clothes.

In addition, the degradation efficiency of powdered TiO_2 was further investigated to evaluate the performance of the fiber. Fig. 6 shows the degradation efficiency of different pollutants by powdered TiO_2, in which the weight was the same as the

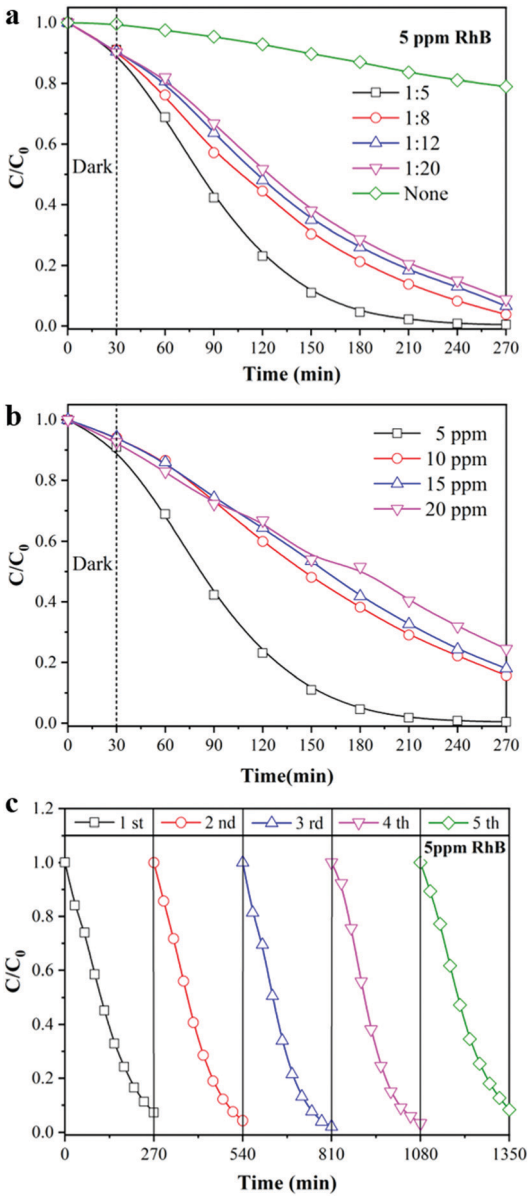

Fig. 5 Photocatalytic degradation of RhB (a) different TiO_2 content; (b) different RhB concentrations; (c) cycle experiment.

TiO_2 content of the 1 : 5 TiO_2/TPU fiber-based textile. Due to the sufficient contact of pollutants with the catalysts, powdered TiO_2 exhibited excellent adsorption and degradation performances. TiO_2/TPU fiber-based textiles could also degrade various contaminants, regardless of whether they were 5 ppm RhB, or 20 ppm RhB or 4-CP. However, there was still a large gap between the degradation ability of the fiber and powder catalyst. Hence, the challenge remained to develop more exposed surfaces of TiO_2 in fiber-based textiles.

Photocatalytic hydrogen production has been widely regarded as a route with good prospects for addressing the current and increasingly serious energy crisis. It is of great practical significance in the preparation of excellent and reusable photocatalytic textiles for photocatalytic H_2 production as

© 2022 The Author(s). Published by the Royal Society of Chemistry

Open Access Article. Published on 11 January 2022. Downloaded on 6/9/2026 3:33:48 PM.
This article is licensed under a Creative Commons Attribution-NonCommercial 3.0 Unported Licence.

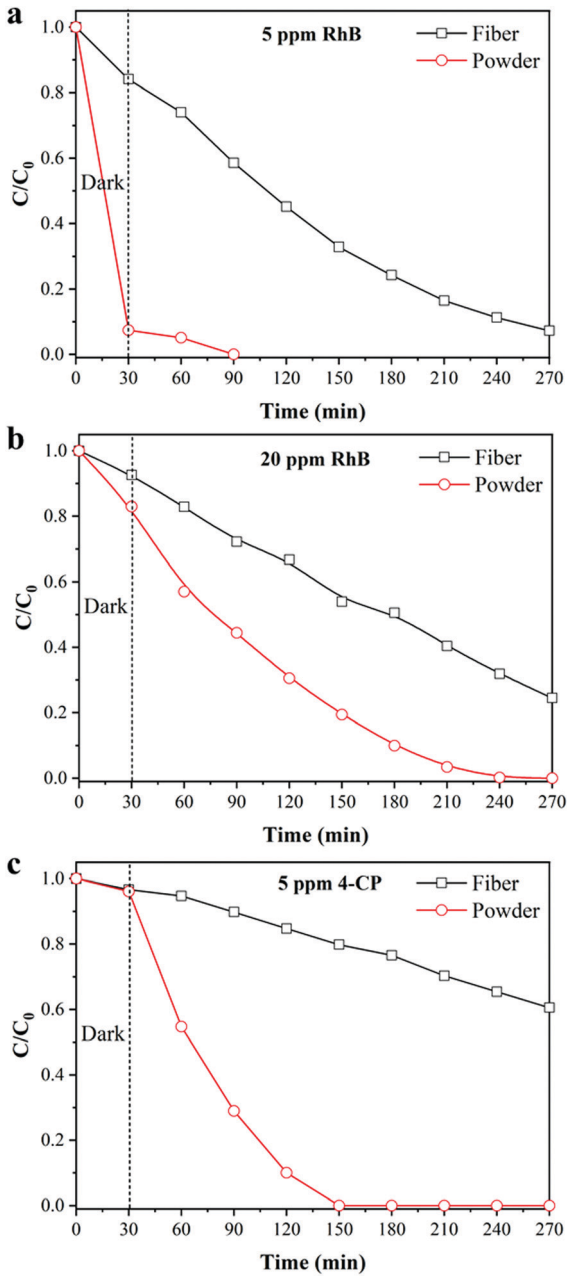

Fig. 6 Photocatalytic degradation of RhB at different concentrations by powder TiO_2: (a) 5 ppm, (b) 20 ppm; (c) photocatalytic degradation of 4-CP.

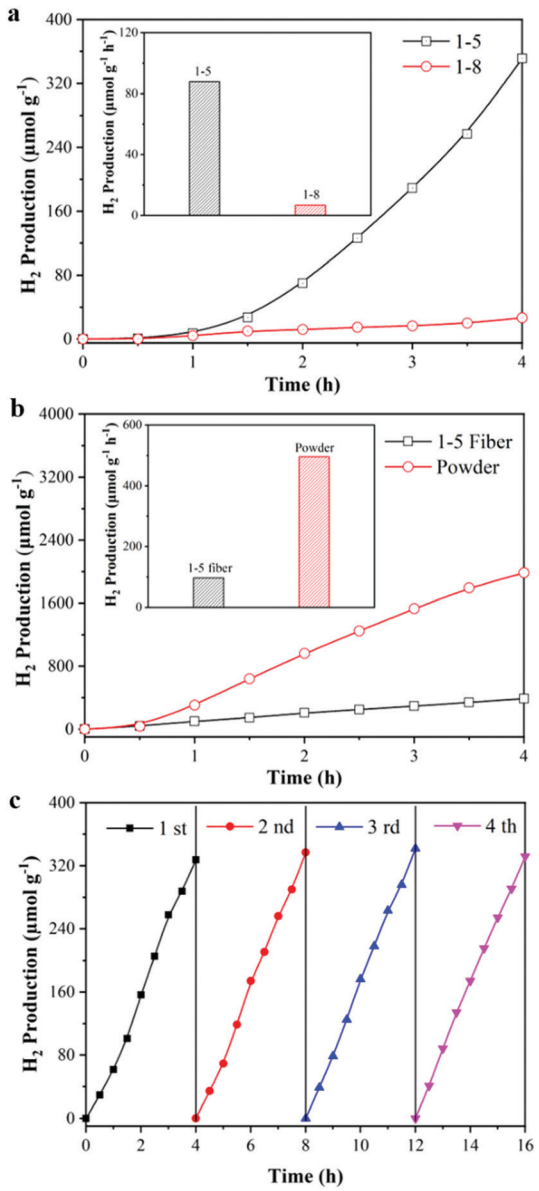

Fig. 7 Photocatalytic H_2 production activity of (a) different TiO_2 content; (b) powdered TiO_2 and (c) cycle experiment.

shown in Fig. S4 (ESI†). As shown in Fig. 7, the performance of the TiO_2/TPU fiber-based textiles was measured by monitoring the amount of hydrogen produced from an aqueous solution containing 10 vol % methanol as the sacrificial agent. The H_2 production rates of fiber-based textiles with different TiO_2 contents are displayed in Fig. 7a. The H_2 production rate of the 1 : 5 TiO_2/TPU fiber-based textile reached 327 μmol g^{-1} after 4 h irradiation, which was 25 times higher than that of the 1 : 8 TiO_2/TPU fiber-based textile. The H_2 production rate of the TiO_2 powder catalyst was further investigated, in which the weight was the same as the TiO_2 content of the 1 : 5 TiO_2/TPU fiber-based textile. As displayed in Fig. 7b, the H_2 production rate of the TiO_2 powder catalyst reached 1984 μmol g^{-1} after 4 h irradiation, which was 6 times higher than that of the fiber-based textile. This was because some TiO_2 was coated with TPU and even agglomerated, which reduced the reaction sites of the catalyst and significantly reduced light utilization. To investigate the stability of the 1 : 5 TiO_2/TPU fiber-based textile for H_2 production, the cycle results are shown in Fig. 7c. Notably, the textile presented highly stable and excellent activity during the cycle tests. Due to greater exposure of TiO_2 during the reaction, the textile performs best in photocatalytic H_2 production during the third cycle, which eventually produces 346 μmol g^{-1}. This result was consistent with the cycle results of photocatalytic degradation. By the way, our fiber-based textile shows

© 2022 The Author(s). Published by the Royal Society of Chemistry

Open Access Article. Published on 11 January 2022. Downloaded on 6/9/2026 3:33:48 PM.
This article is licensed under a Creative Commons Attribution-NonCommercial 3.0 Unported Licence.

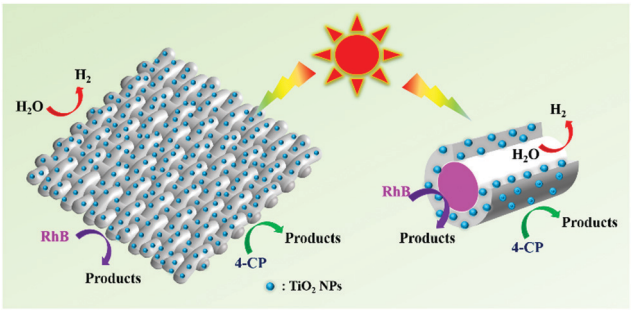

Fig. 8 Proposed mechanism for photodegradation of RhB & 4-CP and photocatalytic H_2 production over hollow composite fiber based smart textiles.

better photocatalytic H_2 production in acidic conditions as shown in Fig. S5 in the ESI.†

From the above measurements, a possible photocatalytic mechanism for our smart textile is briefly proposed in Fig. 8. As we mentioned, TiO_2 NPs are functional elements that enable the photocatalytic properties of the fiber and its textiles. Under light irradiation, excited electrons and holes are generated on TiO_2 NPs on the fiber surface or inner surface, which react with RhB or water for photodegradation and hydrogen production, respectively. The more TiO_2 NPs loaded on the surface or inner surface of the fiber, the higher the photocatalytic performance. Our smart textile is based on hollow composite fibers supporting TiO_2 NPs on its surface as much as possible, which is why our smart textile shows such high photocatalytic performance, as shown in the right of Fig. 8. As shown in Table S1 (ESI†), our smart textile shows better photocatalytic activities than those in other literature, proving composite fiber and its textile are promising candidates to overcome separation and recovery problems of nanostructured catalysts.

Conclusions

In summary, a novel hollow composite fiber composed of TiO_2 and TPU was fabricated *via* a simple wet-spinning method. The fiber exhibits excellent mechanical properties with high tensile strength and elongation at break. In addition, the composite fiber has excellent photocatalytic properties for degradation and hydrogen production. In particular, the 1 : 5 TiO_2/TPU fiber-based textile showed the best photocatalytic performance, in which the removal efficiency of 5 ppm RhB reached 99.6% and the H_2 production rate was 81.75 μmol g^{-1} h^{-1}. In the five-cycle test, the composite fiber showed high stability and excellent activity. The composite fiber showed the best activity in the third cycle, in terms of either degradation performance or hydrogen production performance. This may be due to greater exposure of TiO_2 on the surface of the hollow fibers. Therefore, such smart textiles may open a new avenue for the practical applications of nanostructured catalysts, and we think multifunctional smart textiles will appear to solve environmental issues, such as those smart textiles that combine the removal, degradation, sensing, and detection of pollutants together during practical applications.

Experimental section

Materials

Titanium dioxide nanoparticles (TiO_2 NPs), acetone, *N*,*N*-dimethylformamide (DMF), thermoplastic polyurethanes (TPU), sodium dodecyl sulfate (SDS), methanol, rhodamine B (RhB), p-chlorophenol (4-CP) and chloroplatinic acid ($H_2PtCl_6 \cdot 6H_2O$) were all commercial analytical grade reagents and used as received without any further treatment or purification. Thermoplastic polyurethanes (TPU, Elastollan B 80 A) were obtained from BASF Co. Ltd.

Wet-spinning of TiO_2/TPU fibers

TiO_2/TPU composite fibers were prepared *via* a wet-spinning process, as shown in Scheme 1. In a typical experimental procedure, 0.5 g SDS was dispersed into 15 g DMF solution under sonication for 15 min. Then, 0.125 g TiO_2 was added to the mixed solution under sonication for 50 min. Thereafter, 1.0 g TPU was added and stirred at 98 °C until the solid completely dissolved. After cooling to room temperature, the TiO_2/TPU suspension could be used for the wet-spinning process. The suspension was extruded from a syringe through a 23G needle into an acetone-based coagulation bath. After coagulation, the fibers were continuously collected and dried in air. In this research, the TiO_2-to-TPU weight ratios of the prepared suspensions were 1 : 2, 1 : 5, 1 : 8, 1 : 12 and 1 : 20. Pure TPU fiber was also prepared as a control. To keep the TiO_2 dispersed evenly, the TiO_2-to-SDS weight ratio of the prepared suspensions was 1 : 4. The fibers were woven into a textile (1.5 × 1.5 cm) as the photocatalyst for photocatalytic experiments.

Characterizations

The structure of the composite fibers was investigated by using scanning electron microscopy (SEM, SNE-4500 M Plus). The distribution of elements in the fiber was investigated by using field emission scanning electron microscopy (FE-SEM, Hitachi, SU8220). Stress–strain curves of the composite fibers were obtained by using a TA Instruments Q800 dynamic mechanical analysis (DMA) device.

Photodegradation performances

As a ''green'' wastewater purification technology driven by solar radiation, photocatalysis has been widely used for decomposing organic pollutants into harmless inorganic molecules. The TiO_2/TPU composite fiber was woven into a textile and fixed on a two-line stage to evaluate its photocatalytic performance, such as photodegradation and H_2 production. RhB was used as the model pollutant to evaluate the photodegradation performance of each prepared photocatalyst when illuminated by a 300 W xenon lamp. Typically, the prepared photocatalyst was added to 100 mL of RhB solution. During the photodegradation process, the concentration of RhB solution was measured by a UV-vis

© 2022 The Author(s). Published by the Royal Society of Chemistry

Open Access Article. Published on 11 January 2022. Downloaded on 6/9/2026 3:33:48 PM.
This article is licensed under a Creative Commons Attribution-NonCommercial 3.0 Unported Licence.

spectrophotometer (Jinghua, 754PC) to record the absorbance at 554 nm. The degradation percentage (η) of RhB after photoreaction for t min was then calculated by the following equation: $\eta = (C_0 - C_t)/C_0 \times 100\%$ (C_0 = initial RhB concentration, C_t = residual RhB concentration at t min).

The degradation performance of 4-chlorophenol (4-CP) was further investigated. The prepared pollutant was a 4-CP aqueous solution (5 ppm). The process was the same as that for the photodegradation of RhB. Eventually, the concentration of the 4-CP solution was monitored with high-performance liquid chromatography (Thermo Fisher, Ultimate 3000).

Photocatalytic hydrogen evolution

The H_2 generation experiment was performed in a 150 mL sealed quartz three-necked Pyrex flask, and a 300 W xenon lamp was used as the visible-light source. The photocatalyst was added to 100 mL of methanol (10 vol%, pH = 3) aqueous solution containing H_2PtCl_6 (Pt/TiO_2 = 1 wt%). The oxygen in the reaction system was replaced with argon gas by a vacuum pump. Then, the system was irradiated under the light source. One hundred milliliter gas samples were taken at regular intervals (30 min), and the gas component was analyzed by a gas chromatograph (Fuli 9790II, with Ar as the carrier gas).

Author contributions

Jing Zhang: data curation, investigation, methodology, writing – original draft; Xuan Li and Jian Guo: methodology, validation, visualization; Gengheng Zhou, Li Xiang and Shuguang Wang: conceptualization, data curation, writing – review & editing; Zuoli He: conceptualization, supervision, project administration, funding acquisition, writing – review & editing.

Conflicts of interest

There are no conflicts to declare.

Acknowledgements

This research was supported under the framework of the National Natural Science Foundation of China (No. 22002071), Young Taishan Scholars Program of Shandong Province (No. tsqn. 201909026), Youth Interdisciplinary Science and Innovative Research Groups of Shandong University (Grant No. 2020QNQT014), Future Young Scholars Program of Shandong University (No. 61440089964189). The authors would like to thank Conghua Qi from Shiyanjia Lab (www.shiyanjia.com) for the TEM and XPS analysis. The authors thank S. Wang from The State Key Laboratory of Microbial Technology, Shandong University for his assistance with SEM.

References

1 L. Lin, Z. Lin, J. Zhang, X. Cai, W. Lin, Z. Yu and X. Wang, *Nat. Catal.*, 2020, **3**, 649–655.
2 J. Bian, J. Feng, Z. Zhang, Z. Li, Y. Zhang, Y. Liu, S. Ali, Y. Qu, L. Bai, J. Xie, D. Tang, X. Li, F. Bai, J. Tang and L. Jing, *Angew. Chem., Int. Ed.*, 2019, **58**, 10873–10878.
3 Z. He, C. Kim, L. Lin, T. H. Jeon, S. Lin, X. Wang and W. Choi, *Nano Energy*, 2017, **42**, 58–68.
4 Q. Xiang, B. Cheng and J. Yu, *Angew. Chem., Int. Ed.*, 2015, **54**, 11350–11366.
5 L. Cheng, D. Zhang, Y. Liao, F. Li, H. Zhang and Q. Xiang, *J. Colloid Interface Sci.*, 2019, **555**, 94–103.
6 S. Li, C. Wang, M. Cai, F. Yang, Y. Liu, J. Chen, P. Zhang, X. Li and X. Chen, *Chem. Eng. J.*, 2022, **428**, 131158.
7 J. Wang, Y. Sun, L. Fu, Z. Sun, M. Ou, S. Zhao, Y. Chen, F. Yu and Y. Wu, *Nanoscale*, 2020, **12**, 22030–22035.
8 Z. Chen, H. Yin, C. Wang, R. Wang, Y. Peng, C. You and J. Li, *Environ. Sci. Technol.*, 2021, **55**, 9285–9292.
9 J. Mao, X. An, Z. Gu, J. Zhou, H. Liu and J. Qu, *Environ. Sci. Technol.*, 2020, **54**, 10323–10332.
10 Y. Li, D. Zhang, X. Feng, Y. Liao, Q. Wen and Q. Xiang, *Nanoscale Adv.*, 2019, **1**, 1812–1818.
11 B. Osuagwu, W. Raza, A. B. Tesler and P. Schmuki, *Nanoscale*, 2021, **13**, 12750–12756.
12 A. Nicosia, F. Vento, G. M. Di Mari, L. D'Urso and P. G. Mineo, *Nanomaterials*, 2021, **11**, 400.
13 D. H. K. Murthy, H. Matsuzaki, Q. Wang, Y. Suzuki, K. Seki, T. Hisatomi, T. Yamada, A. Kudo, K. Domen and A. Furube, *Sustainable Energy Fuels*, 2019, **3**, 208–218.
14 F. Li, L. Cheng, J. Fan and Q. Xiang, *J. Mater. Chem. A*, 2021, **9**, 23765–23782.
15 Z. He, C. Kim, T. H. Jeon and W. Choi, *Appl. Catal., B*, 2018, **237**, 772–782.
16 A. C. Marques, M. Vale, D. Vicente, M. Schreck, E. Tervoort and M. Niederberger, *Glob. Chall.*, 2021, **5**, 202000116.
17 K. Ansari, S. Dalela, S. Kumar and N. Chouhan, *Sustainable Energy Fuels*, 2021, **5**, 2545–2562.
18 A. Iqbal, U. Saidu, F. Adam, S. Sreekantan, N. Yahaya, M. N. Ahmad, R. J. Ramalingam and L. D. Wilson, *Molecules*, 2021, **26**(9), 2509.
19 C. Hua, X. Dong, N. Zheng, X. Zhang and M. Xue, *Sustainable Energy Fuels*, 2020, **4**, 6196–6202.
20 H. Wang, Z. Wu, W. Zhao and B. Guan, *Chemosphere*, 2007, **66**, 185–190.
21 M. Gar Alalm, A. Tawfik and S. Ookawara, *J. Environ. Chem. Eng.*, 2016, **4**, 1929–1937.
22 J. Zeng, C. Peng, X. Wang, R. Wang, N. Zhang and S. Xiong, *J. Appl. Polym. Sci.*, 2019, 136.
23 T. Kaur, A. Sraw, R. K. Wanchoo and A. P. Toor, *Sol. Energy*, 2018, **162**, 45–56.
24 M. N. Chong, B. Jin, C. W. K. Chow and C. Saint, *Water Res.*, 2010, **44**, 2997–3027.
25 P. M. Martins, J. M. Ribeiro, S. Teixeira, D. Y. Petrovykh, G. Cuniberti, L. Pereira and S. Lanceros-Méndez, *Materials*, 2019, **12**, 1649.
26 I. Vassalini, J. Gjipalaj, S. Crespi, A. Gianoncelli, M. Mella, M. Ferroni and I. Alessandri, *Adv. Sustainable Syst.*, 2020, **4**, 1900112.

© 2022 The Author(s). Published by the Royal Society of Chemistry

Open Access Article. Published on 11 January 2022. Downloaded on 6/9/2026 3:33:48 PM.
This article is licensed under a Creative Commons Attribution-NonCommercial 3.0 Unported Licence.

27 I. Vassalini, G. Ribaudo, A. Gianoncelli, M. F. Casula and I. Alessandri, *Environ. Sci.: Nano*, 2020, **7**, 3888–3900.
28 Z. He, G. Zhou, J. H. Byun, S. K. Lee, M. K. Um, B. Park, T. Kim, S. B. Lee and T. W. Chou, *Nanoscale*, 2019, **11**, 5884–5890.
29 A. S. More, T. Lebarbé, L. Maisonneuve, B. Gadenne, C. Alfos and H. Cramail, *Eur. Polym. J.*, 2013, **49**, 823–833.
30 P. A. Charpentier, K. Burgess, L. Wang, R. R. Chowdhury, A. F. Lotus and G. Moula, *Nanotechnology*, 2012, **23**, 425606.
31 J. Kasanen, M. Suvanto and T. T. Pakkanen, *Polym. Test.*, 2011, **30**, 381–389.
32 S. Zhang, Z. He, G. Zhou, B. M. Jung, T. H. Kim, B. J. Park, J. H. Byun and T. W. Chou, *Compos. Sci. Technol.*, 2020, **189**, 108011.
33 A. Tewari, S. Gandla, S. Bohm, C. R. McNeill and D. Gupta, *ACS Appl. Mater. Interfaces*, 2018, **10**, 5185–5195.
34 X. Wu, Y. Han, X. Zhang and C. Lu, *ACS Appl. Mater. Interfaces*, 2016, **8**, 9936–9945.
35 J. O. Akindoyo, M. D. H. Beg, S. Ghazali, M. R. Islam, N. Jeyaratnam and A. R. Yuvaraj, *RSC Adv.*, 2016, **6**, 114453–114482.
36 Y. Meng, Y. Zhao, C. Hu, H. Cheng, Y. Hu, Z. Zhang, G. Shi and L. Qu, *Adv. Mater.*, 2013, **25**, 2326–2331.
37 B. Wang, A. Thukral, Z. Xie, L. Liu, X. Zhang, W. Huang, X. Yu, C. Yu, T. J. Marks and A. Facchetti, *Nat. Commun.*, 2020, **11**, 2405.
38 X. Pu, L. Li, M. Liu, C. Jiang, C. Du, Z. Zhao, W. Hu and Z. L. Wang, *Adv. Mater.*, 2016, **28**, 98–105.
39 Z. Li, T. Huang, W. Gao, Z. Xu, D. Chang, C. Zhang and C. Gao, *ACS Nano*, 2017, **11**, 11056–11065.
40 S. W. Finefrock, X. Zhu, Y. Sun and Y. Wu, *Nanoscale*, 2015, **7**, 5598–5602.
41 Z. Jiang, Q. Li, M. Chen, J. Li, J. Li, Y. Huang, F. Besenbacher and M. Dong, *Nanoscale*, 2013, **5**, 6265–6269.
42 S. Zhang, Z. He, G. Zhou, B. M. Jung, T. H. Kim, B. J. Park, J. H. Byun and T. W. Chou, *Compos. Sci. Technol.*, 2020, 189.
43 G. Zhou, J.-H. Byun, Y. Oh, B.-M. Jung, H.-J. Cha, D.-G. Seong, M.-K. Um, S. Hyun and T.-W. Chou, *ACS Appl. Mater. Interfaces*, 2017, **9**, 4788–4797.
44 G. Zhou, Y. Q. Wang, J. H. Byun, J. W. Yi, S. S. Yoon, H. J. Cha, J. U. Lee, Y. Oh, B. M. Jung, H. J. Moon and T. W. Chou, *ACS Nano*, 2015, **9**, 11414–11421.
45 Z. He, J. H. Byun, G. Zhou, B. J. Park, T. H. Kim, S. B. Lee, J. W. Yi, M. K. Um and T. W. Chou, *Carbon*, 2019, **146**, 701–708.
46 X. Xu, P. Fan, J. Ren, Y. Cheng, J. Ren, J. Zhao and R. Song, *Compos. Sci. Technol.*, 2018, **168**, 255–262.

© 2022 The Author(s). Published by the Royal Society of Chemistry